Characterization of the microstructure of hydrazone crosslinked polysaccharide-based hydrogels through rheological and diffusion studies

Materials Science & Engineering C 94 (2019) 1056–1066

Contents lists available at ScienceDirect

Materials Science & Engineering C

journal homepage: www.elsevier.com/locate/msec

Characterization of the microstructure of hydrazone crosslinked polysaccharide-based hydrogels through rheological and diffusion studies

Jennika Karvinen[a,*], Teemu O. Ihalainen[c], Maria Teresa Calejo[a], Ilari Jönkkäri[b], Minna Kellomäki[a,c]

[a] Faculty of Biomedical Sciences and Engineering and BioMediTech Institute, Tampere University of Technology, Tampere FI-33101, Finland
[b] Faculty of Engineering Sciences, Tampere University of Technology, FI-33101 Tampere, Finland
[c] Faculty of Medicine and Life Sciences and BioMediTech Institute, University of Tampere, Tampere FI-33014, Finland

ARTICLE INFO

Keywords:
Microstructure
Hydrogel
Mesh size
Rheometry
FRAP

ABSTRACT

Microstructure plays an essential role in the control of hydrogel properties. It is also an important factor when cells or drugs are encapsulated inside the hydrogel. In this work, the microstructures of hydrazone crosslinked hyaluronan-, alginate- and gellan gum-based hydrogels were evaluated thoroughly for the first time by using rheology- and diffusion (fluorescence recovery after photobleaching, FRAP)-based methods. The effect of gel parameters on the viscoelastic and diffusion properties of hydrogels, and further on their structural parameters (mesh size, average molecular weight of the polymer chain between neighboring crosslinks, crosslinking density) are shown. Results further show that diffusivity decreased when larger dextran sizes were used, which were equivalent to the mesh sizes of hydrogels (15 nm to 47 nm) evaluated by the rheological method. This mesh size range allows the transportation of smaller molecules, but also peptides and most of the proteins. A correlation between the storage modulus and the structural parameters was also shown. Overall, hydrazone crosslinking offers an easy way to produce polysaccharide-based hydrogels with variable microstructures by altering the gel parameters.

1. Introduction

Hydrogels are crosslinked polymeric network materials, that can hold large amounts of water due to their hydrophilic nature. These gels are of particular interest for different tissue engineering (TE) applications due to their favorable properties, such as efficient nutrient diffusion, mechanical and viscoelastic properties, biodegradability and injectability (for easy delivery into tissues). These properties can be easily tuned to achieve biochemical and biophysical properties that resemble native tissues. How suitable the hydrogels are as biomaterials and how well they perform depends greatly on their microstructure. Therefore, it is important to know the structural parameters of the hydrogels, e.g., mesh size, crosslinking density, and the average molecular weight of the polymer chain between neighboring crosslinks.

In TE, the mesh size of the hydrogel plays a critical role in modulating the cellular physiology, since cells (size typically between 7 μm and 15 μm) may encounter physical constraints, if the mesh size (or pore size) is too small [1, 2]. Moreover, an appropriate mesh size is also extremely important for the proper exchange of nutrients and waste products across the polymer network and with the external environment. Therefore, mesh size should be carefully considered and adjusted when cells are encapsulated inside the hydrogel. In consistency, when hydrogels are used as drug delivery systems (DDS), mesh size can significantly affect the loading capacity and the release kinetics of the bioactive species. It is important to notice, however, that mesh size should not be confused with pore size. Pores are larger voids in the structure that typically have a diameter of μm scale. However, pore size positively correlates with mesh size [3-5].

In our previous work, we developed hydrazone crosslinked hyaluronan (HA)- [6, 7], alginate (AL)- [6] and gellan gum (GG)-based [8] hydrogels, that were designed to fulfill the needs of neural [6], corneal stroma [7] and, the general needs of soft tissue applications [8]. Those hydrogels revealed promising properties suitable for these applications, when we characterized their chemical structure, swelling, biodegradation, and the mechanical and optical properties [6-8]. To the best of our knowledge, however, neither the structural parameters nor the diffusion properties of these hydrogels have been determined thoroughly before. Here, we provide a thorough microstructure characterization of these hydrogels by using rheology- and FRAP-based methods. We determined the structural parameters and the diffusion coefficients for

* Corresponding author.
E-mail address: jennika.karvinen@tut.fi (J. Karvinen).

https://doi.org/10.1016/j.msec.2018.10.048
Received 18 April 2018; Received in revised form 5 September 2018; Accepted 11 October 2018
Available online 17 October 2018

these hydrogels. We report our findings in terms of the effect of the gel parameters (polymer components and their degree of substitution (DS %) and molecular weight, ratio of gel components, polymer concentration) on the viscoelastic and diffusion properties of the hydrogels. We further relate our data to the hydrogel microstructure.

2. Materials and methods

2.1. Materials

Synthesis of aldehyde-modified hyaluronan (HALD1-H, HALD1-L, HALD2-H, HALD2-L and HAALD1-L), alginate (ALALD) and gellan gum components (GGALD3 and GGALD4), and hydrazide-modified polyvinyl alcohol (PVAHY) and hyaluronan (HAADH-H, HAADH-L and HACDH-L) components were carried out according to our previously reported procedures [6-8]. The number in the name of the components is related to the variable degree of substitution (DS%) of the polymer, and H or L at the end of the name is related to the different molecular weight (H = high M_w = 1.5-1.8 × 10^6 g/mol and L = low M_w = 1.5 × 10^5 g/mol) of the polymer. Collagen type I from human placenta was purchased from Sigma-Aldrich (St. Louis, MO, USA).

FITC-dextrans with average molecular weight of 20, 150, 500 and 2000 kDa were purchased from TdB Consultancy AB (Uppsala, Sweden). Table 1 shows the hydrodynamic radii of the FITC-dextrans given by the supplier, as well as those calculated based on the equation provided by Hadjiev and Amsden [9],

$$R_h = 0.0163 M_w^{0.52}, \quad (1)$$

where R_h is the hydrodynamic radius and M_w is the molecular weight of solute (dextran).

2.2. Formation of hydrazone crosslinked hydrogel samples

Hydrazone crosslinked polysaccharide-based HA-PVA, AL-PVA, GG-HA and HA-HA(-col I) hydrogels were prepared according to [6-8], by mixing components A and B, as shown in Table 2. The hydrogel codes used in this study are explained in Supplementary Table S1. Briefly, the polymer components were dissolved either in 10% sucrose or in PBS. Gellan gum solutions were heated (50° C) to enable the dissolution, whereas other components were dissolved at room temperature. Components A and B were mixed together at room temperature. Component C (neutralized collagen I) was added to component A prior to mixing. The compositions and gelation times (determined using a tube tilt test [10]) of the hydrogels are presented in Table 2 and the chemical structures of the hydrogels in Fig. 1.

2.3. Rheological measurements of hydrogels

Rheological measurements of hydrogels were performed using a RS150 RheoStress Haake rheometer equipped with Rheowizard 4.3 software (ThermoHaake, Germany) with cone-plate geometry (20 mm diameter, 0.8 mm gap). Equal volumes of component A and B were mixed together to form 500 μL hydrogel in a mold (20 mL cut syringe). The mold was covered with Parafilm and the hydrogels were allowed to gelate for 24 h before being analyzed. Experiments were carried out on three parallel samples. All rheological experiments were performed at 37° C in the oscillatory mode. The test methods used were oscillatory amplitude sweep (γ = 0.01–10, ω = 1 Hz) and frequency sweep (ω = 0.1–10 Hz, γ = 0.03 or 0.1 chosen from the linear viscoelastic region (LVR) based on the amplitude sweep measurement).

Table 1
Hydrodynamic radii of the FITC-dextrans according to supplier (R_{h1}), and as calculated based on the equation provided by Hadjiev and Amsden [9] ($_{h2}$).

Solute	M_w kDa	R_{h1} nm	R_{h2} nm
FD20	20	3.3	2.8
FD150	150	8.5	8.0
FD500	500	14.7	15.0
FD2000	2000	27.0	30.8

The storage modulus (G') represents the elastic behavior of a material, and it is a measure of the deformation energy stored by the material during shear. After removal of the load, the energy is completely available and it acts as a driving force for reformation or it compensates the previous deformation. Thus, the material shows reversible deformation behavior [11]. G' describes how the material responds to shearing strains and can be calculated using the following equation:

$$G' = \frac{\sigma_0}{\gamma_0} cos(\delta), \quad (2)$$

where σ_0 is the stress, γ_0 is the strain amplitude and δ is the phase angle between stress and strain.

The loss modulus (G") represents the viscous behavior of a material, and it is a measure of the deformation energy used by the material during shear (for changing the material structure). Energy-losing materials show irreversible deformation behavior [11]. G" can be calculated using the following equation:

$$G' = \frac{\sigma_0}{\gamma_0} sin(\delta). \quad (3)$$

The complex modulus (G^*) results from the storage and loss moduli, and therefore it characterizes the complete viscoelastic behavior containing both the elastic and viscous portion [11]. G^* can be calculated with the following equation:

$$|G^*| = \sqrt{(G')^2 + (G'')^2}. \quad (4)$$

The loss tangent (tan δ) indicates the overall viscoelasticity of the material, and it is a measure of the ratio of energy lost to energy stored during deformation [12]. tan δ can be calculated from the following ratio:

$$tan\delta = \frac{G''}{G'}. \quad (5)$$

2.3.1. Calculation of the structural parameters

Rheology can be used to evaluate the average mesh size of the hydrogels. The average mesh size (ξ, nm), which is defined as the distance (Å) between the crosslinking points, can be calculated based on the so-called rubber elastic theory (RET) from the following equation:

$$\xi = \left(\frac{G' N_A}{RT}\right)^{-1/3}, \quad (6)$$

where G' is the storage modulus, N_A is the Avogadro constant (6.022 × 10^{23}), R is the gas constant (8.314 J/K mol) and T is the temperature (310 K)[13, 14].

The crosslinking density of the hydrogels can also be evaluated. The crosslinking density (n_e, mol/m^3), which describes the number of elastically active junctions in the network per unit of volume, can be calculated based on the RET from the following equation:

$$n_e = \frac{G_e}{RT}, \quad (7)$$

where G_e is the plateau value of storage modulus measured by frequency sweep test [15].

Rheology also allows the evaluation of the average molecular weight of the polymer chain between neighboring crosslinks (M_c, kg/mol). The M_c in the hydrogel can be calculated with the following equation:

Table 2
Compositions and gelation times of hydrazone-crosslinked HA-PVA, AL-PVA, GG-HA and HA-HA(-col I) hydrogels. The number in the name of the components A is related to variable degree of substitution (DS%) of the polymer, and H or L at the end of the name is related to the different molecular weight (H= high M_w= 1.5-1.8×10^6 g/mol and L= low M_w= 1.5×10^5 g/mol) of the polymer.

Gel #	Code	Component A	DS%	Conc. mg/mL	Component B	DS%	Conc. mg/mL	Component C	Conc. mg/mL	Mass ratio A:B(:C)	Vol. ratio A:B(:C)	Polymer conc. %	Gelation Time
1	HP1	HALD1-H	5	20	PVAHY	13	10	-	-	2:1	1:1	1.5	seconds
2	HP1a	HALD1-H	5	10	PVAHY	13	5	-	-	2:1	1:1	0.75	1-5 min
3	HP1b	HALD1-H	5	5	PVAHY	13	2.5	-	-	2:1	1:1	0.375	5 min
4	HP2	HALD2-H	9	25	PVAHY	13	5	-	-	5:1	1:1	1.5	seconds
5	HP3	HALD1-L	5	20	PVAHY	13	10	-	-	2:1	1:1	1.5	seconds
6	HP4	HALD2-L	9	20	PVAHY	13	10	-	-	2:1	1:1	1.5	seconds
7	AP	ALALD	7	20	PVAHY	13	10	-	-	2:1	1:1	1.5	1-5 min
8	GH1	GGALD3	20	20	HAADH-H	30	10	-	-	2:1	1:1	1.5	5 min
9	GH2	GGALD3	20	20	HAADH-L	50	10	-	-	2:1	1:1	1.5	5 min
10	GH3	GGALD4	25	15	HAADH-H	30	15	-	-	1:1	1:1	1.5	5 min
11	GH4	GGALD4	25	15	HAADH-L	50	15	-	-	1:1	1:1	1.5	5 min
12	HH1	HALD2-L	9	20	HAADH-L	50	10	-	-	2:1	1:1	1.5	5 min
13	HH2	HAALD1-L	15	30	HACDH-L	17	30	-	-	1:1	1:1	3	5 min
14	HH2C	HAALD1-L	15	30	HACDH-L	17	30	Collagen I	5	12:12:1	2:2:1	2.5	5 min

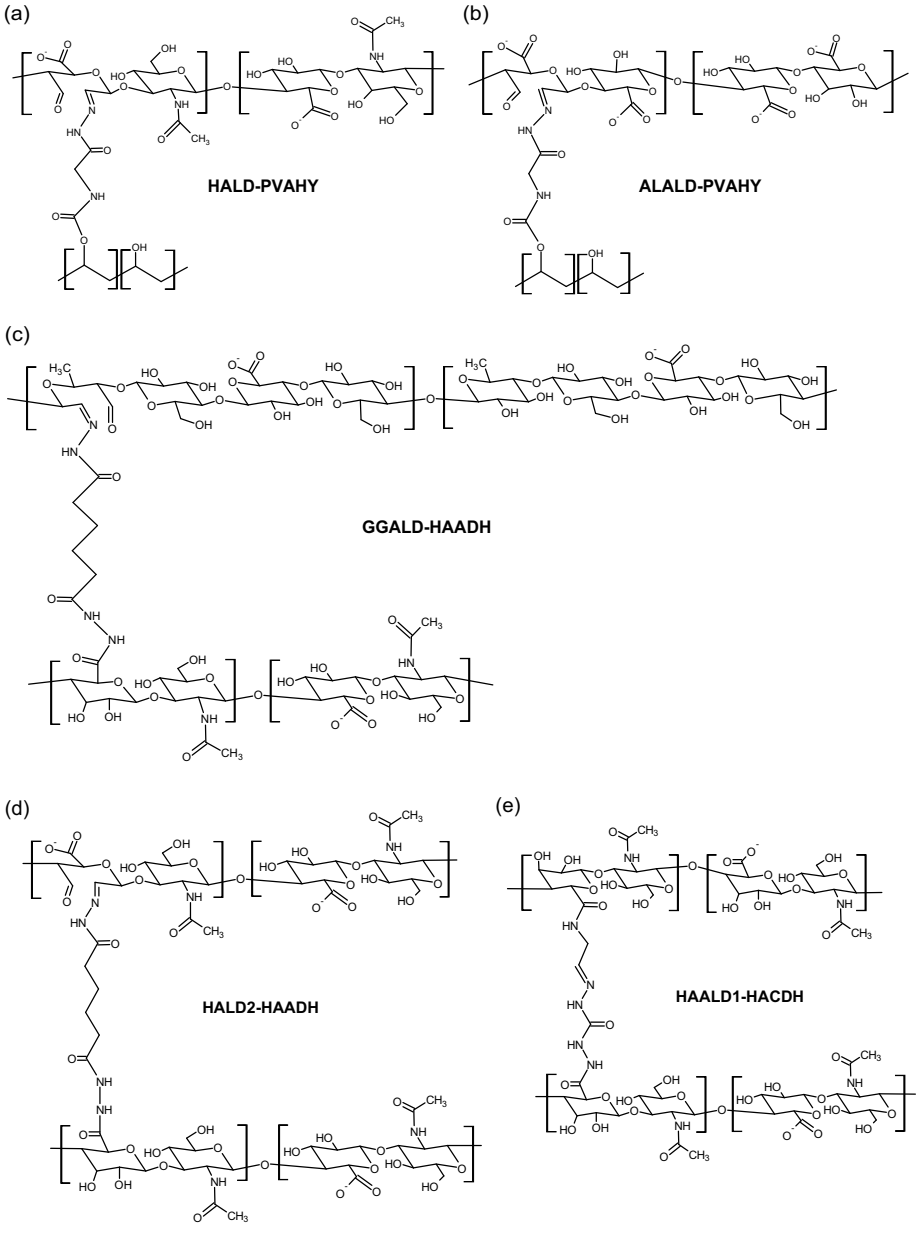

Fig. 1. Chemical structures of hydrazone crosslinked polysaccharide-based (a) HA-PVA, (b) AL-PVA, (c) GG-HA and (d,e) HA-HA hydrogels.

$$M_c = \frac{c\rho RT}{G_e}, \quad (8)$$

where c is the polymer concentration (0.0375–1.5 % w/v) and ρ is the density of water at 310 K (993 kg/m^3) [16].

2.4. Studying diffusion in hydrogels using the fluorescence recovery after photobleaching technique

2.4.1. FRAP experiments

FRAP experiments were performed using a Zeiss LSM780 Laser Scanning Confocal Microscope (Carl Zeiss, Germany) and a Plan-Apochromat 63x/1.2 water immersion objective (Carl Zeiss, Germany). A few hours before the experiment, equal volumes of components A and B were mixed together to form 200 μL hydrogel samples in a mold (10 mL cut syringe). FITC-dextran particles (20, 150, 500 or 2000 kDa) were mixed with the gel components in the dark prior to gelation to obtain 0.5 mg/mL dextran concentration per hydrogel. Hydrogel samples were placed on a 35 mm Glass Bottom Microwell Dish (MatTek Corporation, USA) and were analyzed at room temperature. Images were taken at a constant depth of 100 μm from the bottom of the dish. A sequence of 250 frames was captured with an image size of 256 × 256 pixels and a pixel size of 264 nm. FRAP bleach pulse was set to happen after 5 frames at a circular region of interest (ROI), which had a width of 20 pixels. In the bleaching process, the 488 nm Argon laser intensity was set to 100% and imaging was carried out using a laser intensity of 2%. FITC was excited at 488 nm and emission was detected in the range of 496 nm to 650 nm. Five parallel FRAP experiments were conducted with each hydrogel containing different sized dextrans.

ImageJ was used to construct an average shape and intensity profile of the ROI. The FRAP data were then exported to Excel (Microsoft, Redmond, USA). The normalization of the data was performed according to [17].

2.4.2. Half maximum

The half maximums ($\tau_{1/2}$) were determined from the FRAP-curves. $\tau_{1/2}$ can be considered as the index for the speed of recovery, and it is defined as the time it takes for the curve to reach 50% of the plateau fluorescence intensity level (Supplementary Fig. S2). The shorter the $\tau_{1/2}$, the faster the recovery. The use of this parameter has, however, been criticized [18]. In our study, $\tau_{1/2}$ was only one of the parameters used to compare the hydrogels.

2.4.3. Virtual cell modeling

FRAP recoveries were modeled with Virtual Cell software [19]. The hydrogel was simulated by a 50 μm x 50 μm square with a pixel size of 0.2 μm. The time step of the simulation was set to 10 ms, and images were collected at 250 ms intervals. The bleaching of the fluorescent dextran due to confocal imaging was simulated by a laser light induced continuous mass action reaction that was focused on a 36 μm x 36 μm sized square region in the middle of the gel. The bleach pulse ROI of 400 ms was approximated to correspond in geometry and size to the one in the FRAP experiments. The length of the bleach pulse was adjusted to 400 ms, as in the FRAP experiments. The imaging time of one frame on the confocal microscope was about 200 ms, and with the bleaching ROI being in the middle of the image, it was assumed that the bleach region was imaged about 100 ms after the bleach. This value was also used in the simulations as the first recovery image time point. The diffusion constant of dextran was adjusted until the model fitted with the measured data. The reaction map is shown in Supplementary Fig. S1.

2.4.4. Percent recovery

In addition to the specified half maximums and diffusion coefficients, the percent recoveries were determined from the FRAP-curves. The FRAP recovery curve does not always reach the original level of fluorescence intensity. Some of the bleached molecules are immobile within the FRAP ROI; they neither contribute to the recovery nor give away sites for incoming un-bleached molecules. The curve can therefore be divided into immobile and mobile fractions (Supplementary Fig. S2.). The percent recovery tells how much light returns relative to the amount of light that was there before the photobleaching, and it can be determined from the following equation:

$$\%recovery = \left(\frac{Y}{X}\right) \times 100\%, \quad (9)$$

where Y is the amount of fluorescence that returns to the bleached area and X is the amount of fluorescence lost due to photobleaching (Supplementary Fig. S2).

2.5. Statistical data analysis

Statistical data analyses were performed with MATLAB (Statistics and Machine Learning Toolbox™). All the quantitative data are presented as mean and standard deviation. A non-parametric Kruskal-Wallis test and a Wilcoxon rank sum test were used to determine whether there were statistically significant differences within the rheological and FRAP data set and to analyze specific sample pairs, respectively. Due to a relatively low n, non-parametric testing was chosen. Bonferroni correction was used when more than two groups were compared. A p-value of < 0.05 was considered significant.

3. Results

3.1. Evaluation of structural parameters of hydrogels using rheology

3.1.1. Amplitude and frequency sweep measurements

Amplitude sweep measurements were performed with a RS150 RheoStress Haake rheometer with cone-plate geometry. The measurements were performed at variable amplitudes (strain) by keeping the frequency constant in order to determine the LVR of the hydrogels. The amplitude dependence of the moduli calculated for HA-PVA and AL-PVA hydrogels are presented in Fig. 2, whereas for GG-HA and HA-HA(-col I) hydrogels the curves have already been shown in [7] and [8], respectively. All hydrogels showed a linear behavior of G' up to about 10% strain. Outside the LVR, G' decreases indicating structure breakdown due to large deformations. Many biological materials, unlike most hydrogels, stiffen with higher strains to prevent large deformations. In line with this, none of the hydrogels showed any strain stiffening behavior.

The frequency sweep measurements were performed at variable frequencies at the LVR strain amplitude determined earlier. The frequency dependence of moduli and the phase angle tan δ of HA-PVA and AL-PVA hydrogels are presented in Fig. 2 and Fig. 3. Corresponding curves for GG-HA and HA-HA(-col I) hydrogels have been presented earlier in [8] and [7], respectively. For all hydrogels, G' was higher than G" (elastic response is stronger than the viscous one) and independent of frequency (for the measuring range 0.1 Hz to 10 Hz). G' was also parallel to G". The ratio of G" to G' (tan δ) was < 0.1 for all hydrogels, and therefore their structures were considered to be strong. Due to these observations, these hydrogels were considered as stable and strongly crosslinked gels. Results also showed that G' increased at higher frequencies for some gels. This stiffening and more solid-like behavior is caused by the inability of longer polymer chains to rearrange in the given time scale [12].

The G', G" and G* of the hydrogels presented in Table 3 were determined at 0.1 Hz to 1 Hz. The results showed that the G' (and G*) of HA-PVA hydrogels decreased when the polymer concentration and DS% of the HALD-component decreased, or when the molecular weight of HA increased. With GG-HA hydrogels, the G' (and G*) increased when the DS% of the HAADH-component increased, or when the hydrogel

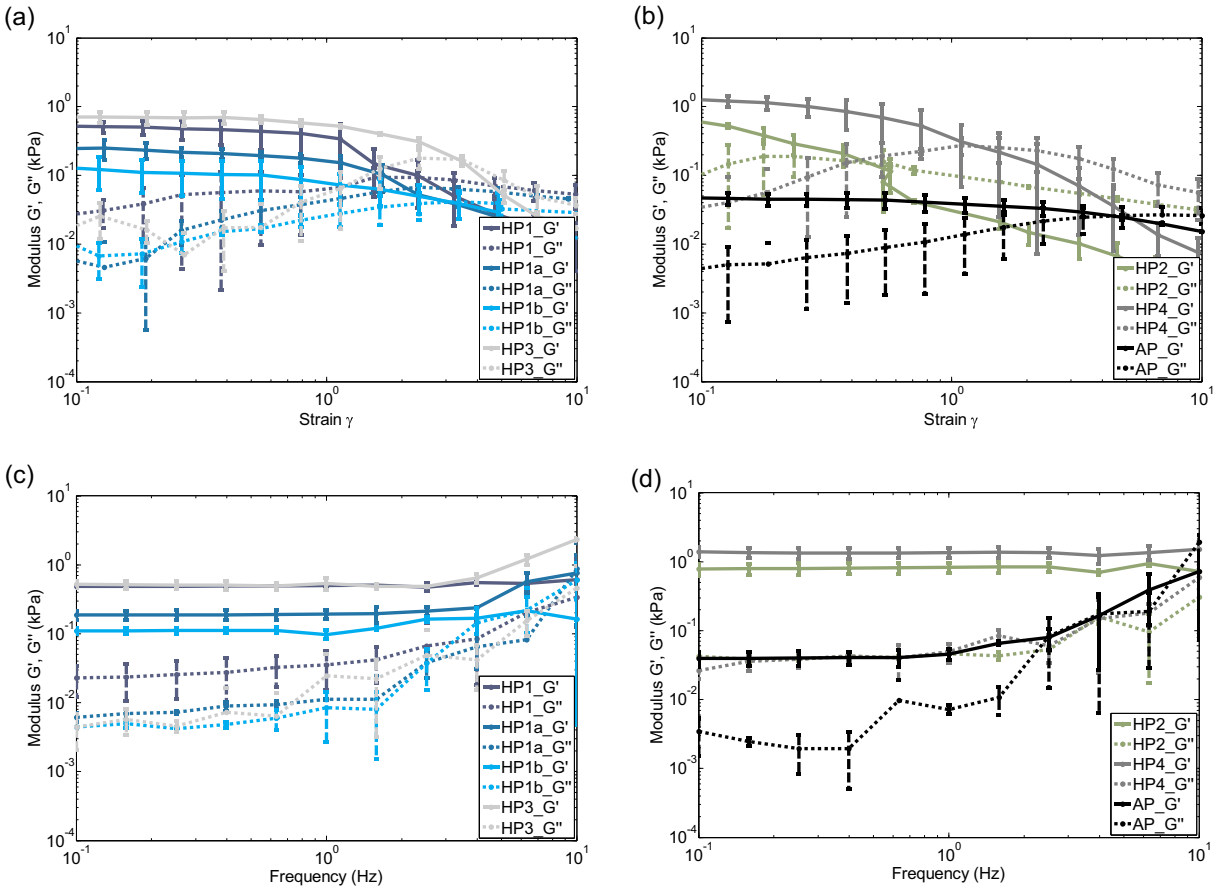

Fig. 2. Rheological properties of hydrazone crosslinked hydrogels. Amplitude (a,b) and frequency (c,d) dependence of moduli of hydrazone crosslinked HA-PVA and AL-PVA hydrogels. The mean (n = 3) and standard deviation bars are shown.

mass ratio was 1:1 compared with a mass ratio of 2:1. The G' (and G*) of HA-HA(-col I) hydrogels were close to the G' (and G*) of HA-PVA and GG-HA hydrogels. The G' (and G*) increased when the polymer concentration of the HA-HA hydrogel increased. The addition of collagen into the hydrogel further increased the G' (and G*) leading to the highest G' (and G*) among all the hydrogels. The AP hydrogel differed significantly from the others and showed the lowest G' (and G*) of all. The hydrogels can be arranged according to decreasing G' (and G*) in the following order: HHAC > HP4 > HH2 > HP2 > GH4 > HH1 > HP3 > HP1 > GH2 > GH3 > GH1 > HP1a > HP1b > AP. The G" followed this order with some minor exceptions. Overall, hydrogels with higher G' were considered to have higher resilience to deformation.

3.1.2. Evaluation of average mesh size, crosslinking density and average molecular weight of the polymer chain between neighboring crosslinks of hydrogels

The average mesh sizes (ξ) and average molecular weights of the polymer chain between neighboring crosslinks (M_c) of the hydrogels were calculated using Eqs. (6) and 8. The calculated parameters are presented in Table 3. The ξ of the hydrogels varied from 14.7 ± 0.8 nm to 47.4 ± 3.4 nm, whereas the M_c of the hydrogels varied from 27.3 ± 1.3 kg/mol to 857.8 ± 146.8 kg/mol. The ξ and M_c of HA-PVA hydrogels decreased when the polymer concentration or the DS% of the HALD-component increased, or when the molecular weight of HA decreased. With GG-HA hydrogels, the ξ and M_c slightly decreased when the DS% of the HAADH-component increased, or when the hydrogel mass ratio was 1:1 compared with a mass ratio of 2:1. The ξ and M_c of HA-HA(-col I) hydrogels were also close to the ξ and M_c of HA-PVA and GG-HA hydrogels. The comparison of HA-HA hydrogels was not easy due to the different compositions used, but overall the mesh size decreased with increased polymer concentration of the hydrogel. Also, the addition of collagen into the gel decreased the mesh size even more. This hydrogel showed the lowest ξ and M_c of all the hydrogels. The HH1 hydrogel was also compared with HP4 and GH2 hydrogels since the hydrogels contained either the same HALD2-L component (HP4) or HAADH-L component (GH2). The ξ and M_c of the HH1 hydrogel were higher than for the HP4 hydrogel and lower than for the GH2 hydrogel. Compared with other hydrogels, the mesh size of the AP hydrogel differed significantly from others and showed the highest ξ and M_c of all. The hydrogels can be arranged according to increasing ξ and M_c, as follows: HHAC < HP4 < HH2 < HP2 < GH4 < HH1 < HP3 < HP1 < GH2 < GH3 < GH1 < HP1a < HP1b < AP.

The crosslinking densities (n_e) of the hydrogels were calculated using Eq. (7). The calculated parameters are shown in Table 3. The n_e of the hydrogels varied from 0.016 ± 0.004 mol/m^3 (1.6 × 10^{-20} mol/μm^3) to 0.526 ± 0.085 mol/m^3 (5.26 × 10^{-19} mol/μm^3). The n_e of HA-PVA hydrogels decreased when the polymer concentration of the hydrogel or the DS% of the HALD-component decreased, or when the molecular weight of HA increased. The n_e of GG-HA hydrogels slightly increased when the DS% of the HAADH-component increased, or when the hydrogel mass ratio was 1:1 compared with a mass ratio of 2:1. The n_e of HA-HA(-col I) hydrogels were close to the n_e of HA-PVA and GG-HA hydrogels. The n_e increased with the increased polymer concentration of the HA-HA hydrogel. The addition of collagen into the hydrogel increased the n_e even more leading to the highest n_e among all the hydrogels. When the HH1 hydrogel was compared with similar HP4 and GH2 hydrogels, the n_e of the HH1 hydrogel was lower than for the HP4 hydrogel and higher than for the GH2 hydrogel. The AP hydrogel differed significantly from the others and showed the lowest n_e of all. The hydrogels can be arranged according to decreasing n_e, as follows:

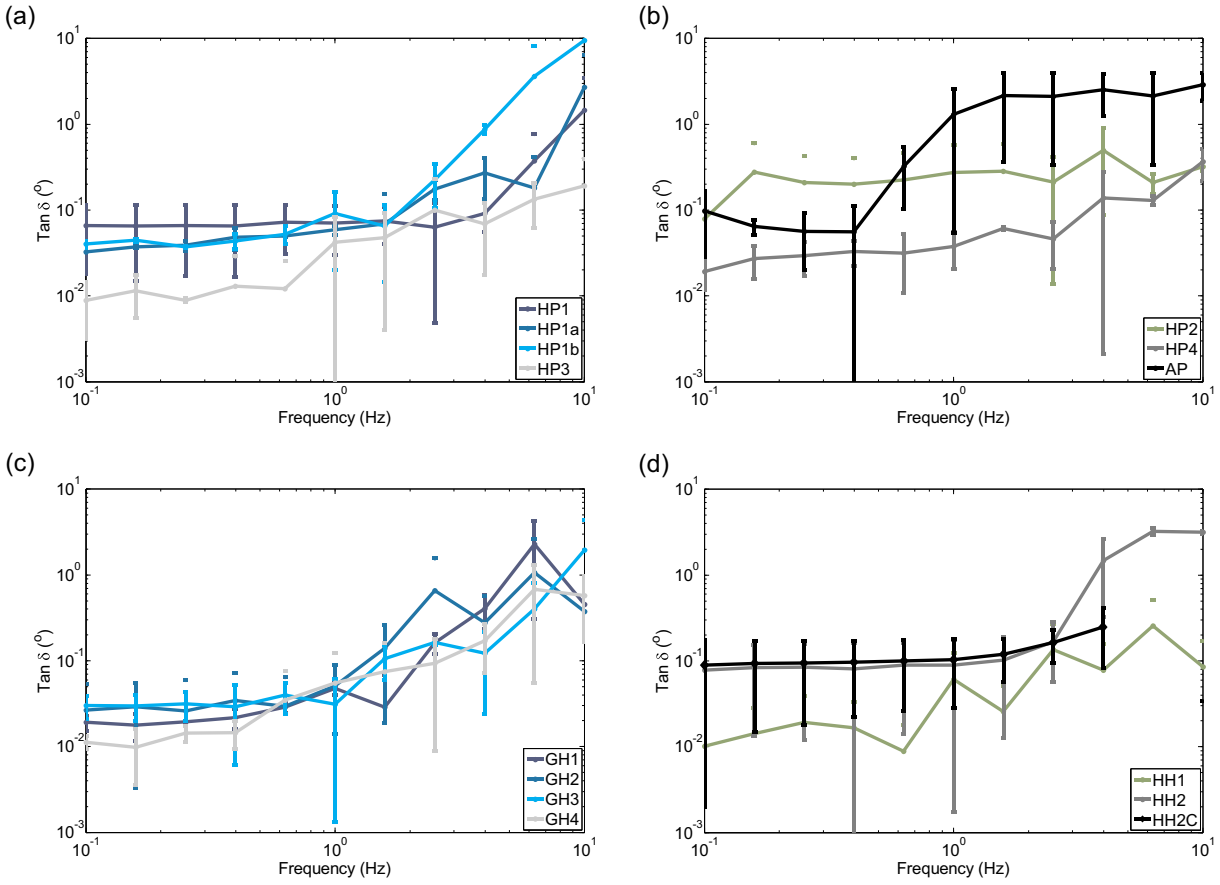

Fig. 3. Frequency dependence of phase angle tan δ of hydrazone crosslinked (a,b) HA-PVA, (c) AL-PVA, (d) GG-HA and (e) HA-HA(-colI) hydrogels. The mean (n = 3) and standard deviation bars are shown.

HHAC > HP4 > HH2 > HP2 > GH4 > HH1 > HP3 > HP1 > GH2 > GH3 > GH1 > HP1a > HP1b > AP.

3.2. Studying the diffusion in hydrogels with the FRAP technique

The FRAP technique was used to study diffusion within the hydrogels. The recovery kinetics of fluorescein labeled dextrans (FITC-dextran) after photobleaching light pulse were measured by using confocal laser scanning microscopy. The normalized fluorescence recovery curves of different sized FITC-dextrans (20, 150, 500 and 2000 kDa) in hydrazone crosslinked HP1, AP, GH4 and HH2C hydrogels are shown in Fig. 4, whereas for other HA-PVA, GG-HA and HA-HA hydrogels they are shown in Supplementary Fig. S3-A and -B. Microscopy time-lapse images corresponding to different phases of the FRAP experiment are presented next to the curves.

The half maximums ($\tau_{1/2}$) were determined from the FRAP-curves (Fig. 5). Shorter $\tau_{1/2}$ indicates faster recovery. In the case of HA-PVA hydrogels (Fig. 5 (a)), the recovery was faster with HP1-based

Table 3
Parameters of hydrazone crosslinked hydrogels determined based on the rheological frequency sweep analysis. Storage moduli (G'), loss moduli (G"), complex moduli (G^*), average mesh sizes (ξ), average crosslinking densities (n_e) and average molecular weights of the polymer chain between neighboring crosslinks (M_c) of the hydrazone crosslinked HA-PVA, AL-PVA, GG-HA and HA-HA(-colI) hydrogels. The mean (n = 3) and standard deviation are shown. There were no statistically significant differences found between the hydrogels.

Gel #	Code	G' Pa	G" Pa	G^* Pa	ξ nm	n_e mol/m^3	M_c kg/mol
1	HP1	491 ± 5	28 ± 15	492 ± 5	20.6 ± 0.1	0.190 ± 0.002	78.2 ± 0.8
2	HP1a	189 ± 29	8 ± 1	189 ± 29	28.4 ± 1.5	0.073 ± 0.011	206.4 ± 32.0
3	HP1b	109 ± 11	5 ± 2	109 ± 11	34.0 ± 1.2	0.042 ± 0.004	354.6 ± 36.0
4	HP2	804 ± 15	42 ± 3	805 ± 15	17.5 ± 0.1	0.312 ± 0.006	47.8 ± 0.9
5	HP3	514 ± 71	9 ± 1	514 ± 72	20.3 ± 0.9	0.199 ± 0.028	75.7 ± 10.5
6	HP4	1355 ± 219	39 ± 11	1355 ± 218	14.7 ± 0.8	0.526 ± 0.085	28.8 ± 4.7
7	AP	41 ± 2	4 ± 3	41 ± 3	47.1 ± 0.8	0.016 ± 0.001	937.9 ± 45.8
8	GH1	259 ± 2	7 ± 3	259 ± 2	25.5 ± 0.1	0.100 ± 0.001	148.2 ± 1.1
9	GH2	352 ± 4	9 ± 4	352 ± 4	23.0 ± 0.1	0.137 ± 0.002	109.1 ± 1.2
10	GH3	335 ± 7	10 ± 10	335 ± 7	23.4 ± 0.2	0.130 ± 0.003	114.6 ± 2.4
11	GH4	618 ± 10	14 ± 11	619 ± 10	19.1 ± 0.1	0.240 ± 0.004	62.1 ± 1.0
12	HH1	568 ± 59	12 ± 4	569 ± 59	19.6 ± 0.7	0.220 ± 0.023	68.1 ± 7.1
13	HH2	805 ± 232	56 ± 45	809 ± 223	17.5 ± 1.8	0.312 ± 0.090	47.7 ± 15.2
14	HH2C	1442 ± 197	142 ± 11	1418 ± 160	14.4 ± 0.7	0.559 ± 0.076	27.0 ± 3.7

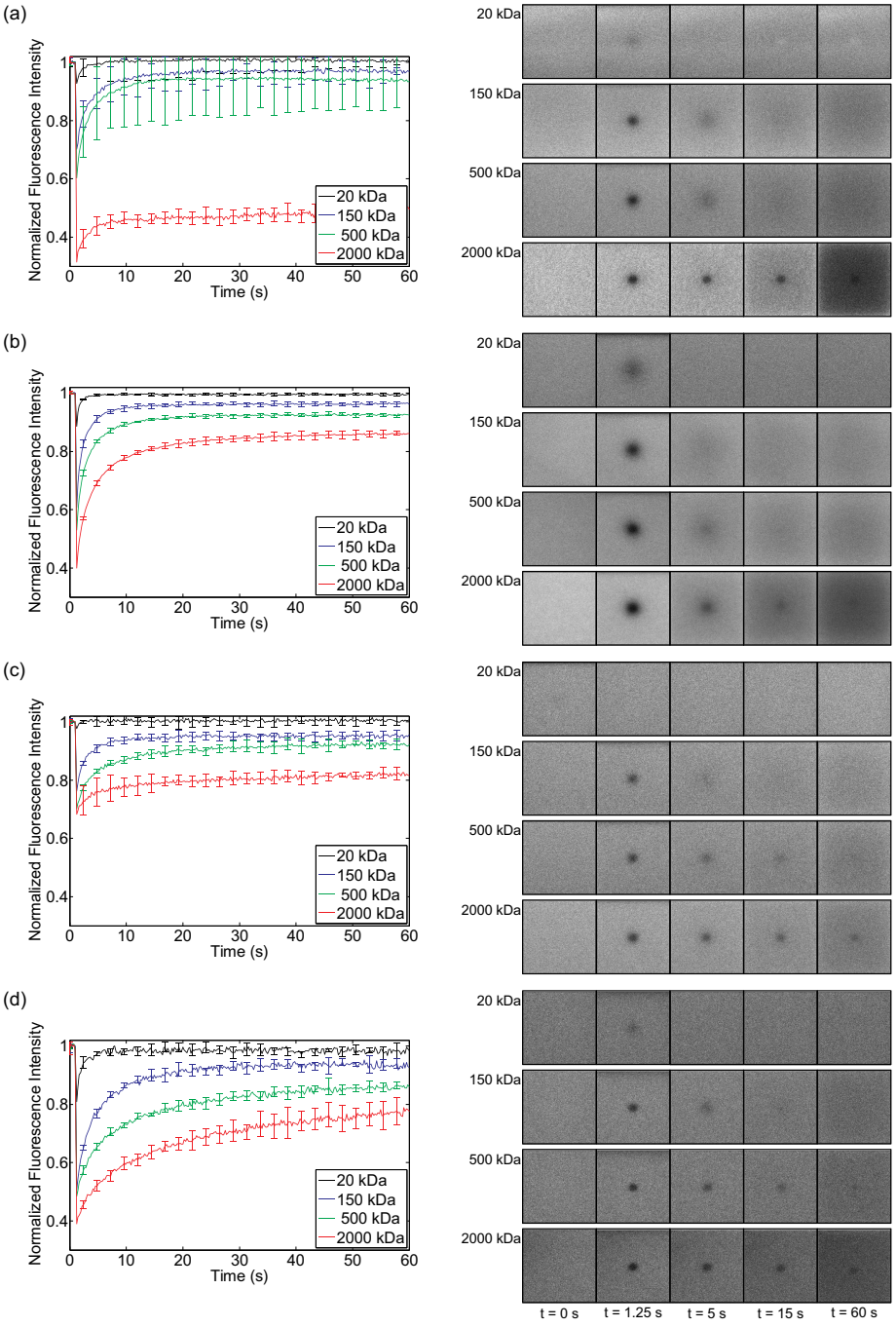

Fig. 4. FRAP experiments of hydrazone crosslinked hydrogels. Normalized fluorescence recovery curves of different sized FITC-dextrans (20, 150, 500 and 2000 kDa) in (a) HP1, (b) AP, (c) GH4 and (d) HH2C hydrogels. Microscopy time-lapse images corresponding to different phases of the FRAP experiment are presented next to the curves. The curves of other hydrogels are shown in the Supplementary Fig. S3-A and -B. The mean (n = 5) and standard deviation bars are shown.

hydrogels when compared with the others. Also, the recovery was faster when the polymer concentration of the HP1-hydrogel decreased. With GG-HA hydrogels (Fig. 5 (b)), the recovery was slower when the DS% of the HAADH- or GGALD-component increased. In the case of HA-HA hydrogels (Fig. 5 (b)), the recovery was slower when the polymer concentration increased, as well as when collagen was added. When the HH1 hydrogel was compared with similar HP4 and GH2 hydrogels, the recovery in the HP4 hydrogel was faster, whereas in the GH2 hydrogel it was the opposite. The recovery in the AP hydrogel (Fig. 5 (a)) was faster than in HP2, HP3, HP4, GG-HA, HA-HA hydrogels, but slower than in HP1-based hydrogels. The recovery in GG-HA hydrogels was slower when compared with HA-PVA and AP-hydrogels, but faster when compared with HA-HA hydrogels. The recovery in HA-HA hydrogels was slower compared with HA-PVA and AP hydrogels.

Since the use of half maximum in the FRAP quantification has been criticized (because it also depends on the geometry and the size of the bleached region) [18], more accurate Virtual Cell (VCell) modeling was used to simulate the fluorescence recovery kinetics. The diffusion coefficients were determined by fitting the simulated recovery kinetics with the measured FRAP data. The diffusion coefficients of FITC-dextrans in different hydrogels are presented in Table 4. Overall, the diffusion coefficient decreased with increasing dextran size. With 20 kDa dextrans, the diffusion coefficients in certain HA-PVA hydrogels (HP1a, HP1b) were close to that of water. When the dextran size was larger, the

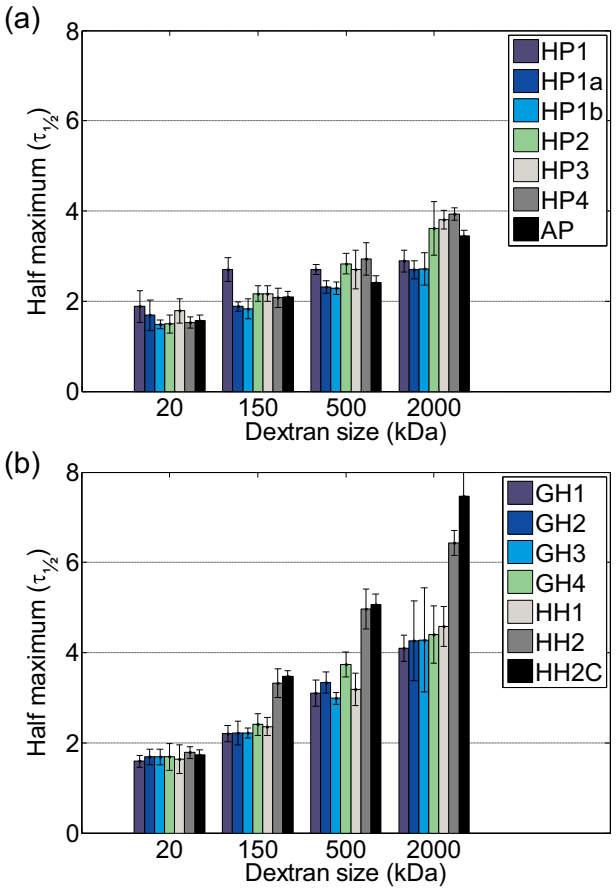

Fig. 5. Half maximums ($\tau_{1/2}$) determined in hydrazone crosslinked (a) HA-PVA and AL-PVA, (b) GG-HA, and HA-HA(-colI) hydrogels based on the normalized fluorescence recovery curves of different sized FITC-dextrans (20, 150, 500 and 2000 kDa).

Table 4
Diffusion coefficients of FITC-dextrans incorporated inside the hydrazone crosslinked hydrogels determined based on FRAP analysis and VCell modeling. Comparable theoretical values of diffusion coefficients of FITC-dextrans in water are calculated according to Brandl et al. [20]. The mean (n = 5) and standard deviation are shown. The p-values are shown in the Supplementary Table S2-A-D.

Gel #	Code	Diffusion coefficient $\mu m^2/s$			
		20 kDa	150 kDa	500 kDa	2000 kDa
1	HP1	30 ± 4	2.0 ± 0.4	0.75 ± 0.18	0.05 ± 0.03
2	HP1a	75 ± 2	8.0 ± 1.2	1.50 ± 1.00	0.25 ± 0.04
3	HP1b	80 ± 4	10.0 ± 1.4	2.00 ± 0.13	0.25 ± 0.05
4	HP2	50 ± 1	2.0 ± 0.5	0.75 ± 0.18	0.10 ± 0.07
5	HP3	60 ± 8	2.0 ± 0.4	0.75 ± 0.04	0.10 ± 0.01
6	HP4	50 ± 4	2.0 ± 0.4	1.00 ± 0.18	0.10 ± 0.02
7	AP	45 ± 5	10.0 ± 0.4	2.00 ± 0.22	0.50 ± 0.01
8	GH1	40 ± 1	3.0 ± 0.7	0.50 ± 0.05	0.25 ± 0.01
9	GH2	40 ± 4	2.0 ± 0.6	0.25 ± 0.18	0.10 ± 0.01
10	GH3	40 ± 4	3.0 ± 0.1	0.75 ± 0.01	0.10 ± 0.06
11	GH4	40 ± 4	2.0 ± 0.1	0.25 ± 0.01	0.10 ± 0.04
12	HH1	55 ± 3	5.0 ± 0.1	1.00 ± 0.25	0.25 ± 0.01
13	HH2	40 ± 5	1.0 ± 0.5	0.20 ± 0.06	0.05 ± 0.02
14	HH2C	35 ± 4	0.8 ± 0.1	0.10 ± 0.02	0.05 ± 0.01
	Water	81	28	15	7

diffusion coefficients decreased significantly and were far from that of water (Table 4). The results presented are based on the diffusion coefficients determined for the larger dextran sizes since those sizes

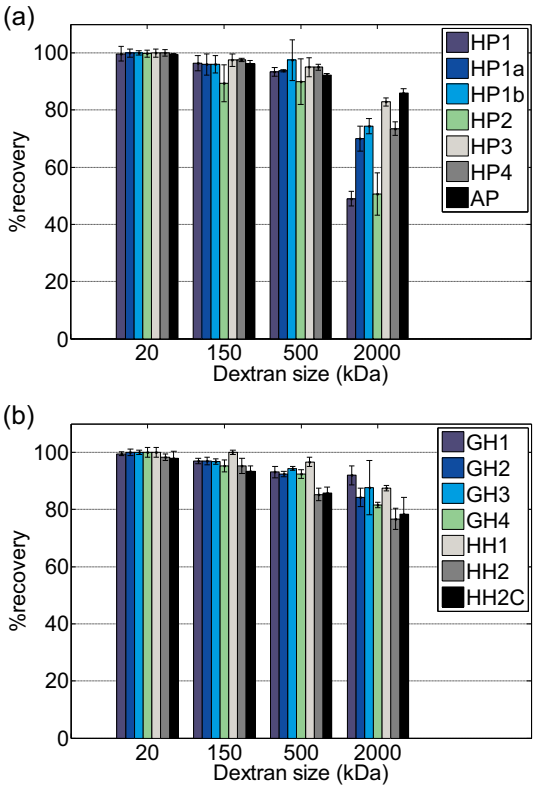

Fig. 6. Percent recoveries determined in hydrazone crosslinked (a) HA-PVA and AL-PVA, (b) GG-HA, and HA-HA(-colI) hydrogels based on the normalized fluorescence recovery curves of different sized FITC-dextrans (20, 150, 500 and 2000 kDa).

were more interesting considering the possible restrictions. When HA-PVA hydrogels were compared, the diffusion coefficients increased when the polymer concentration of hydrogel was lower. The change in the M_w or DS% of the HALD-component did not significantly affect the diffusion coefficient. The change in the DS% of the HAADH- or GGALD-component of GG-HA hydrogels did not affect the diffusion coefficient either. In HA-HA hydrogels, the diffusion coefficient was lower when the polymer concentration was increased. The addition of collagen did not have a significant effect. When the HH1 hydrogel was compared with similar HP4 and GH2 hydrogels, the diffusion coefficients of dextrans in the HH1 hydrogel were higher in both cases. Similar diffusion coefficient values were found for dextrans in HA-PVA, HA-HA and GG-HA hydrogels, whereas in AP hydrogel the diffusion coefficient was the highest among all the hydrogels. Overall, the difference between the hydrogels became less pronounced when the size of the dextrans increased because the hydrogels started to restrict the diffusion of dextran molecules.

The percent recoveries, also termed mobile fractions, were determined from the FRAP-curves and they are shown in Fig. 6. Higher percent recovery indicates a larger mobile fraction. In the case of HA-PVA hydrogels (Fig. 6 (a)), the mobile fraction was larger when the polymer concentration of the HP1-hydrogel or the M_w of the HALD-component were lower. When the DS% of the high molecular weight HALD-component was increased or when the DS% of the low molecular weight HALD-component was decreased, the mobile fraction was larger. In GG-HA hydrogels (Fig. 6 (b)), the mobile fraction was smaller when the DS% of the HAADH- or GGALD-component increased. In the case of HA-HA hydrogels (Fig. 6 (b)), the mobile fraction was smaller when the polymer concentration was increased. Compared with similar HP4 and GH2 hydrogels, the mobile fraction in the HH1 hydrogel was larger. The mobile fraction in the AP hydrogel was close to that in GG-HA and HA-HA hydrogels, but slightly larger than that in HA-PVA

hydrogels. Overall, the difference between the hydrogels was not so prominent when the size of the dextrans increased. The recovery was almost 100% when smaller dextran sizes were used, but as the dextran size increased, the curves failed to reach the original level.

4. Discussion

Hydrazone crosslinked polysaccharide-based hydrogels studied in this work have been designed to fulfill the needs of soft tissue applications. HA-PVA and AL-PVA hydrogels have been previously tested with human pluripotent stem cell-derived neuronal cells [6], and they have shown to serve as 3D supportive and biomimicking materials for neural cell culture. HA-HA-based hydrogels, on the other hand, have shown to be suitable for the delivery of hASCs for regeneration of the corneal stroma, as they were previously tested with human adipose derived stem cells (hASCs) [7]. Even though GG-HA-based hydrogels have not yet been tested with any cells, their properties have shown to be promising for the general needs of soft tissue applications [8]. It is common knowledge that a proper transportation of small molecules, such as nutrients is needed for TE applications. Therefore, mesh size also has a critical role in modulating the cellular phenotype, proliferation and ECM production [1]. Knowing the microstructure and diffusion properties of these hydrogels is thus extremely important.

The exact analysis of hydrogel microstructure using common imaging methods is difficult. For example, a Scanning Electron Microscope (SEM) requires dehydration of samples. Drying methods, such as freeze drying, may damage the hydrogel structure [21], and therefore the images are not representative of the actual microenvironment. Therefore, it was necessary to use more suitable techniques. Here, rheology-based method and FRAP were shown to be suitable methods for our hydrogels. The structural parameters could be determined from the wet samples without any destructive drying. The structural parameters of hydrogels were determined by rheology. Data obtained from the rheological measurements not only provided knowledge about the viscoelastic character of hydrogels, but it was also used to determine these parameters. A hydrogel, as a natural rubber, is assumed to fully recover rapidly into its original dimension after being subjected to a relatively small deformation. The so-called rubber elastic theory (RET) allows the approximation of these parameters from the storage modulus of the hydrogel based on the affine network model [13]. FRAP, on the other hand, is an advanced technique that enables the quantification of the diffusion of fluorescent molecules by following the recovery of the fluorescence to a photobleached region in a sample [22-25]. FRAP has been widely used for the study of cells, but it has increasingly been used for the study of hydrogels as well. In FRAP, a short light pulse is used to bleach the fluorescence in a certain region in the sample. This is then followed by the measurement of the recovery of the fluorescence due to the exchange of fluorescent and non-fluorescent molecules between the bleached region and its surroundings. The diffusion rates can be determined based on the fluorescence recovery kinetics [26]. The rate of fluorescence recovery is proportional to the rate of diffusion of the fluorescently labeled molecules. In the case of hydrogels, the diffusion rate correlates with the mesh size of the hydrogel [1]. Thus, FRAP can also be used to estimate the mesh size of the hydrogels.

The RET allows us to investigate the network structure of these hydrogels with rheology. The mesh size, crosslinking density and M_c were calculated for the hydrogels. It should be noted, however, that these parameters give only a raw estimation of the structure [13, 16]. The results shown in Table 3 were in line with the expected outcome that the higher the G' (and the higher the second order elastic constant [6-8]), the lower the mesh size and M_c, and the higher the crosslinking density. In the case of HA-PVA-based hydrogels, smaller mesh size and M_c, and higher crosslinking density were attained by lowering the molecular weight of HA component, or by increasing the DS% of HALD-component or the polymer concentration of hydrogel. With GG-HA-based hydrogels, smaller mesh size and M_c, and higher crosslinking density were achieved by increasing the DS% of HAADH-component or by using the mass ratio of 1:1 (compared with 2:1). With HA-HA-based hydrogels, the smaller mesh size and M_c, and higher crosslinking density were attained by adding collagen.

It is known that both geometrical constraints and possible binding events can retain the diffusion of molecules. The FRAP results showed that the recovery was more complete with smaller dextran molecules (20 kDa and 150 kDa), whereas with larger dextrans (500 kDa and 2000 kDa) the recovery was only partial. The diffusion coefficients also support these findings. The diffusion coefficients decreased significantly as the dextran size increased. In this study, we used molecules that would not show any binding interactions with hydrogel components. Therefore, it was expected that the retained diffusion shown by the results was due to steric hindrance, rather than actual binding between the molecules and the hydrogel. For example, the crosslinking sites can form microregions in the structure, where the polymer is precipitated in certain areas, and these heterogeneities can distort the diffusion results. Also, the size of the solute in relation to the size of the openings between polymer chains, as well as polymer chain mobility can also affect the movement of the solute [27]. In the case of HA-PVA-based hydrogels, the diffusion coefficients increased when the molecular weight of HA-component, DS% of HALD-component or the polymer concentration of hydrogel decreased. The results are reasonable, since these gel parameters lead to larger mesh sizes and decreased crosslinking densities. Similarly, in GG-HA-based hydrogels, higher diffusion coefficients were attained by lowering the DS% of HAADH-component. In HA-HA-based hydrogels, addition of collagen decreased the diffusion coefficients presumably due to additional crosslinking.

The results from the FRAP experiment fit well to the mesh sizes evaluated by the rheological experiments. As expected, the diffusivity decreased significantly with larger dextran sizes (hydrodynamic radii of dextrans: 20 kDa = 2.8 nm, 150 kDa = 8.0 nm, 500 kDa = 15.0 nm, 2000 kDa = 30.8 nm), which were equivalent to the average mesh sizes of the hydrogels (15 nm to 47 nm) determined by the rheological method. The mesh sizes of these hydrazone crosslinked hydrogels are comparable with many other (biological) hydrogels, since most hydrogels have a mesh size ranging from 5 nm to 100 nm [28]. This size range allows the flow of small molecules, for example, nutrients, small-molecule drugs and growth factors, whereas penetration or release of non-covalently entrapped larger molecules may be hindered [29]. Nevertheless, since the average protein size within human cells is about 50 kDa (a sphere with a diameter of less than 6 nm to 7 nm), most proteins should diffuse through the gel, not to mention peptides that are much smaller in size. How fluids and small molecules move inside the hydrogel depends on the diffusion, whereas degradation plays a larger role in the later movement of the cells and large molecules. For example, because water (2 Å) can easily diffuse in and out of the hydrogels, it can increase the hydrolysis and contribute to the degradation of the hydrogel structure [3]. Mesh size or degradation are not the only factors that affect the release from the hydrogels. For example, the release is influenced by how the molecule is incorporated and its specific polarity and size [3].

We have previously tested the HA-PVA and AL-PVA hydrogels reported in this work with human pluripotent stem cell-derived neuronal cells [6]. The results showed that the neuronal spreading and 3D neural network formation is enhanced inside the softest HA-PVA and AL-PVA hydrogels (AP and HP1-based hydrogels) that had brain-mimicking mechanical properties at low strains. Those hydrogels were obtained by using higher molecular weight HA and lower DS% of HALD-component, as well as lower polymer concentration of the hydrogel (HP1-based). The calculated structural parameters and FRAP results support these findings. AP and HP1-based hydrogels had the largest mesh sizes and M_cs, and lowest crosslinking densities, as well as the highest diffusion coefficients of these gel types. This indicates that their microenvironment is more suitable for the cells in terms of better small molecule transportation properties, compared with the other HA-PVA-based

hydrogels tested. When lower molecular weight HA and higher DS% of HALD-component were used, hydrogels were characterized by smaller mesh size and M_c, higher crosslinking density and lower diffusion coefficient. Those gels (HP2, HP3 and HP4 hydrogels) were less-supportive in terms of cell growth and neurite outgrowth along the hydrogel surface (they were not further tested in 3D culturing experiments). We have also previously tested the HA-HA-based hydrogels reported in this work with hASCs [7]. Especially, HH2-based hydrogels were shown to be suitable for the delivery of hASCs for regeneration of the corneal stroma. Directly after encapsulation, all gels showed good hASC survival, but only the collagen-containing HH2C hydrogel showed cells with elongated morphology, and significantly higher metabolic activity compared with the HH2 hydrogel. Even so, HH2C hydrogel was characterized by a lower diffusion coefficient, smaller mesh size and M_c, and higher crosslinking density. In this case, it is likely that the preference of the cells for this hydrogel is related with the presence of the extracellular matrix protein, which contributed to create a biomimetic environment, thereby increasing cell adhesion and proliferation. This effect was likely more pronounced than the contribution of the structural parameters of the gel. It should be noted, however, that the inferior stability of HH1 hydrogel (degraded during the three days of culture, while HH2-based hydrogels remained more stable for the culture period of seven/ten days), which can be related to its adipic acid dihydrazide (ADH)-modification (compared with the carbodihydrazide (CDH)-modification of HH2-based gels), as well as its larger mesh size and M_c and lower crosslinking density, made the comparison more difficult. Moreover, the rheological data of the studied hydrogels showed a linear behavior of G' up to about 10% strain which should be suitable for soft TE applications, since cells and tissues in the human body are seldom subjected to strains larger than 5%.

To the best of our knowledge, the structural parameters or diffusion properties of these particular types of hydrogels have not been studied thoroughly before. Therefore, our gels can mainly be compared with similarly crosslinked HA-HA-based hydrogels presented by Oommen et al. [30], for which they have determined the mesh sizes and M_cs using a similar rheological method. Even though the polymer concentrations or ratios of components are not the same, the results were in line with each other. Since the FRAP experiments have not been conducted with similar types of hydrogels, a direct comparison of results was not possible. Comparison, for example, with PEG-based hydrogels studied by Brandl et al. [20] shows, however, that the diffusion coefficients of similar sized FITC-dextrans are of the same magnitude.

Overall, the results successfully showed that rheology- and FRAP-based methods are appropriate tools to characterize the microstructure of these polysaccharide-based hydrazone crosslinked hydrogels. The results showed that hydrazone crosslinking offers an easy way to produce polysaccharide-based hydrogels with variable microstructures and hence also variable rheological and diffusion properties. These properties were attained by altering the polymer component and the type of its modification, molecular weight and degree of modification, as well as the polymer concentration of the hydrogel and the ratio of polymer components.

5. Conclusions

To conclude, knowledge of the microstructure of hydrogels, especially mesh size, is important to be able to evaluate their suitability as biomedical materials. In this work, the microstructures of the hydrazone crosslinked polysaccharide-based HA-, GG- and AL-based hydrogels were thoroughly characterized for the first time by using rheology- and FRAP-based methods. Also, by using these methods, the microstructure can be evaluated from wet samples, which gives more reliable results than, for example, by imaging dried samples. The results obtained from the rheological and FRAP experiments supported each other. The diffusivity decreased when larger dextran sizes (500 kDa and 2000 kDa) where used. These molecule sizes are equivalent to the average mesh sizes of hydrogels (15 nm to 47 nm) determined by the rheological method, and this mesh size range is comparable with many other hydrogels. Peptides and most of the proteins should be able to freely diffuse through the gel, since their size does not exceed the average mesh size of the gels. The results also showed the expected outcome that the higher the G', the lower the mesh size and M_c, and the higher the crosslinking density. Overall, hydrazone crosslinking offers an easy way to produce polysaccharide-based hydrogels with variable microstructures and variable viscoelastic and diffusion properties by altering the polymer components and their molecular weight and degree of modification, as well as the polymer concentration of hydrogels and the ratio of components.

Acknowledgments

This work was supported by TEKES (the Finnish Funding Agency for Innovation) Human spare parts project. The authors acknowledge Tampere Imaging Facility (TIF) for their service.

Appendix A. Supplementary data

Supplementary data to this article can be found online at https://doi.org/10.1016/j.msec.2018.10.048.

References

[1] S. Lin, N. Sangaj, T. Razafiarison, C. Zhang, S. Varghese, Influence of physical properties of biomaterials on cellular behavior, Pharm. Res. 28 (6) (2011) 1422–1430.
[2] E. Santos, R.M. Hernández, J.L. Pedraz, G. Orive, Novel advances in the design of three-dimensional bio-scaffolds to control cell fate: translation from 2D to 3D, Trends Biotechnol. 30 (6) (2012) 331–341.
[3] E.R. Aurand, K.J. Lampe, K.B. Bjugstad, Defining and designing polymers and hydrogels for neural tissue engineering, Neurosci. Res. 72 (3) (2012) 199–213.
[4] M.C. LaPlaca, V.N. Vernekar, J.T. Shoemaker, D.K. Cullen, Three-dimensional Neuronal Cultures, Methods in Bioengineering: 3D Tissue Engineering, Artech House, Norwood, MA, 2010, pp. 187–204.
[5] B.V. Slaughter, S.S. Khurshid, O.Z. Fisher, A. Khademhosseini, N.A. Peppas, Hydrogels in regenerative medicine, Adv. Mater. 21 (32-33) (2009) 3307–3329.
[6] J. Karvinen, T. Joki, L. Ylä-Outinen, J.T. Koivisto, S. Narkilahti, M. Kellomäki, Soft hydrazone crosslinked hyaluronan- and alginate-based hydrogels as 3D supportive matrices for human pluripotent stem cell derived neuronal cells, React. Funct. Polym. 124 (2018) 29–39.
[7] L. Koivusalo, J. Karvinen, E. Sorsa, I. Jönkkäri, J. Väliaho, P. Kallio, T. Ilmarinen, S. Miettinen, H. Skottman, M. Kellomäki, Hydrazone crosslinked hyaluronan-based hydrogels for therapeutic delivery of adipose stem cells to treat corneal defects, Mater. Sci. Eng. C 85 (2018) 68–78.
[8] J. Karvinen, J.T. Koivisto, I. Jönkkäri, M. Kellomäki, The production of injectable hydrazone crosslinked gellan gum-hyaluronan-hydrogels with tunable mechanical and physical properties, J. Mech. Behav. Biomed. Mater. 71 (2017) 383–391.
[9] N.A. Hadjiev, B.G. Amsden, An assessment of the ability of the obstruction-scaling model to estimate solute diffusion coefficients in hydrogels, J. Control. Release 199 (2015) 10–16.
[10] ASTM Standard F2900:2011, Standard Guide for Characterization of Hydrogels used in Regenerative Medicine, ASTM International, West Conshohocken, PA, USA, 2011.
[11] T.G. Mezger, The Rheology Handbook: For Users of Rotational and Oscillatory Rheometers, Vincentz Network GmbH & Co KG, 2006.
[12] M.J. Moura, M.M. Figueiredo, M.H. Gil, Rheological study of genipin cross-linked chitosan hydrogels, Biomacromolecules 8 (12) (2007) 3823–3829.
[13] P.B. Welzel, S. Prokoph, A. Zieris, M. Grimmer, S. Zschoche, U. Freudenberg, C. Werner, Modulating biofunctional starPEG heparin hydrogels by varying size and ratio of the constituents, Polymers 3 (1) (2011) 602–620.
[14] M. Rubinstein, R.H. Colby, Polym. Phys. 23 Oxford University Press, New York, 2003.
[15] R. Suriano, G. Griffini, M. Chiari, M. Levi, S. Turri, Rheological and mechanical behavior of polyacrylamide hydrogels chemically crosslinked with allyl agarose for two-dimensional gel electrophoresis, J. Mech. Behav. Biomed. Mater. 30 (2014) 339–346.
[16] S. Piskounova, R. Rojas, K. Bergman, J. Hilborn, The effect of mixing on the mechanical properties of hyaluronan-based injectable hydrogels, Macromol. Mater. Eng. 296 (10) (2011) 944–951.
[17] T. Kühn, T.O. Ihalainen, J. Hyväluoma, N. Dross, S.F. Willman, J. Langowski, M. Vihinen-Ranta, J. Timonen, Protein diffusion in mammalian cell cytoplasm, PLoS One 6 (8) (2011) e22962.
[18] C. Klein, F. Waharte, Analysis of Molecular Mobility by Fluorescence Recovery after Photobleaching in Living Cells, Microscopy: Science, Technology, Applications and Education, Formatex Research Center, 2010, pp. 772–783.

[19] B.M. Slepchenko, L.M. Loew, Chapter one-use of virtual cell in studies of cellular dynamics, Int. Rev. Cell Mol. Biol. 283 (2010) 1–56.
[20] F. Brandl, F. Kastner, R.M. Gschwind, T. Blunk, J. Teßmar, A. Göpferich, Hydrogel-based drug delivery systems: comparison of drug diffusivity and release kinetics, J. Control. Release 142 (2) (2010) 221–228.
[21] C. García-González, M. Alnaief, I. Smirnova, Polysaccharide-based aerogels—promising biodegradable carriers for drug delivery systems, Carbohydr. Polym. 86 (4) (2011) 1425–1438.
[22] M. Henke, F. Brandl, A.M. Goepferich, J.K. Tessmar, Size-dependent release of fluorescent macromolecules and nanoparticles from radically cross-linked hydrogels, Eur. J. Pharm. Biopharm. 74 (2) (2010) 184–192.
[23] C. Cha, J.H. Jeong, J. Shim, H. Kong, Tuning the dependency between stiffness and permeability of a cell encapsulating hydrogel with hydrophilic pendant chains, Acta Biomater. 7 (10) (2011) 3719–3728.
[24] E. Schuster, A.-M. Hermansson, C. Öhgren, M. Rudemo, N. Lorén, Interactions and diffusion in fine-stranded β-lactoglobulin gels determined via FRAP and binding, Biophys. J. 106 (1) (2014) 253–262.
[25] M. McGill, J.M. Coburn, B.P. Partlow, X. Mu, D.L. Kaplan, Molecular and macroscale analysis of enzyme-crosslinked silk hydrogels for rational biomaterial design, Acta Biomater. 63 (2017) 76–84.
[26] T.K. Meyvis, S.C. De Smedt, P. Van Oostveldt, J. Demeester, Fluorescence recovery after photobleaching: a versatile tool for mobility and interaction measurements in pharmaceutical research, Pharm. Res. 16 (8) (1999) 1153–1162.
[27] B. Amsden, Solute diffusion within hydrogels. Mechanisms and models, Macromolecules 31 (23) (1998) 8382–8395.
[28] J. Li, D.J. Mooney, Designing hydrogels for controlled drug delivery, Nat. Rev. Mater. 1 (2016) 16071.
[29] D.J. Mooney, R.S. Langer, Engineering biomaterials for tissue engineering: the 10-100 micron size scale, in: B. Palsson, J.A. Hubbell, R. Plonsey, J.D. Bronzino (Eds.), Tissue Engineering, in: chap. 11, CRC Press, 2000, pp. 11-1–11-6.
[30] O.P. Oommen, S. Wang, M. Kisiel, M. Sloff, J. Hilborn, O.P. Varghese, Smart design of stable extracellular matrix mimetic hydrogel: synthesis, characterization, and in vitro and in vivo evaluation for tissue engineering, Adv. Funct. Mater. 23 (10) (2013) 1273–1280.